JACS
JOURNAL OF THE AMERICAN CHEMICAL SOCIETY

ARTICLE

pubs.acs.org/JACS

Planarization of B_7^- and B_{12}^- Clusters by Isoelectronic Substitution: AlB_6^- and AlB_{11}^-

Constantin Romanescu,[†] Alina P. Sergeeva,[‡] Wei-Li Li,[†] Alexander I. Boldyrev,*[,‡] and Lai-Sheng Wang*[,†]

[†]Department of Chemistry, Brown University, Providence, Rhode Island 02912, United States

[‡]Department of Chemistry and Biochemistry, Utah State University, Logan, Utah 84322, United States

Supporting Information

ABSTRACT: Small boron clusters have been shown to be planar from a series of combined photoelectron spectroscopy and theoretical studies. However, a number of boron clusters are quasiplanar, such as B_7^- and B_{12}^-. To elucidate the nature of the nonplanarity in these clusters, we have investigated the electronic structure and chemical bonding of two isoelectronic Al-doped boron clusters, AlB_6^- and AlB_{11}^-. Vibrationally resolved photoelectron spectra were obtained for AlB_6^-, resulting in an accurate electron affinity (EA) for AlB_6 of 2.49 ± 0.03 eV. The photoelectron spectra of AlB_{11}^- revealed the presence of two isomers with EAs of 2.16 ± 0.03 and 2.33 ± 0.03 eV, respectively. Global minimum structures of both AlB_6^- and AlB_{11}^- were established from unbiased searches and comparison with the experimental data. The global minimum of AlB_6^- is nearly planar with a central B atom and an AlB_5 six membered ring, in contrast to that of B_7^-, which possesses a C_{2v} structure with a large distortion from planarity. Two nearly degenerate structures were found for AlB_{11}^- competing for the global minimum, in agreement with the experimental observation. One of these isomers with the lower EA can be viewed as substituting a peripheral B atom by Al in B_{12}^-, which has a bowl shape with a B_9 outer ring and an out-of-plane inner B_3 triangle. The second isomer of AlB_{11}^- can be viewed as an Al atom interacting with a B_{11}^- cluster. Both isomers of AlB_{11}^- are perfectly planar. It is shown that Al substitution of a peripheral B atom in B_7^- and B_{12}^- induces planarization by slightly expanding the outer ring due to the larger size of Al.

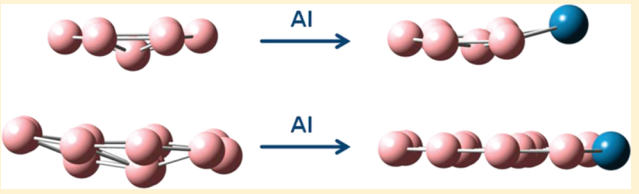

INTRODUCTION

Elemental boron possesses many complex crystal structures consisting of B_{12} icosahedral or larger cage building blocks.[1,2] However, early theoretical calculations suggested that the cage structures are not stable as isolated units in the gas phase and planar or quasiplanar structures are more favored.[3−8] Over the past decade, we have combined photoelectron spectroscopy (PES) and theoretical calculations in a major research effort to elucidate the structure and bonding in small boron clusters.[9−21] We have found that the planarity of boron clusters is primarily due to 2D electron delocalizations, which have given rise to concepts of σ- and π-aromaticity, σ- and π-antiaromaticity, or conflicting aromaticity−antiaromaticity.[11,12,22−24] One of the key structural and bonding features that have emerged from our joint experimental and computational investigations is that each planar boron cluster contains an outer boron ring with strong classical two-center two electron (2c−2e) B−B bonds and various inner B atom groups that are bonded to the outer ring via delocalized σ and π bonding.[9−21] Among the well characterized boron clusters, some are found to be perfectly planar, whereas others are quasiplanar with the inner atoms exhibiting some degree of nonplanarity. A question arises: what causes the nonplanarity?

Some nonplanarity has been traced to antiaromaticity, that is electronic in origin. One aspect that has not been addressed is if the nonplanarity can be mechanical in origin, that is, the outer B ring is too small to fit the central atoms. Two quasiplanar clusters may belong to this category, B_7^- and B_{12}^-. The global minimum of B_7^- is of C_{2v} symmetry with a central B atom significantly out of plane.[15] However, the B_8 cluster is a perfect planar cluster with a B_7 ring and a central B atom.[11] B_{12} is a highly stable and aromatic cluster with a large HOMO−LUMO gap, as revealed from the PES spectra of B_{12}^-.[12] Yet, the global minima of both B_{12} and B_{12}^- are nonplanar and have bowl shapes with an outer B_9 ring and an inner out-of-plane B_3 triangle. In both B_7^- and B_{12}^-, there is a possibility that the outer B rings are simply too small to host the central atoms in a perfect planar arrangement, even though from an electronic point of view planarity clearly favors electron delocalization in two dimensions. Thus, if the outer ring can be expanded to release the strain, we expect that both B_7^- and B_{12}^- should favor the perfect planar structures.

In this article, we set out to test the above hypothesis by substituting a B atom with Al in B_7^- and B_{12}^-. Because of the larger size of Al, it may induce planarity by slightly expanding the outer ring. We have obtained well-resolved photoelectron spectra of AlB_6^- and AlB_7^- at several detachment laser wavelengths. Unbiased global minimum searches are carried out for both

Received: February 9, 2011
Published: April 26, 2011

ACS Publications © 2011 American Chemical Society

dx.doi.org/10.1021/ja2012438 | J. Am. Chem. Soc. 2011, 133, 8646–8653

clusters to locate their lowest energy structures, which are then compared with the experimental data. It is shown that indeed the Al atom can induce planarization in both clusters.

Relatively little is known about metal-doped boron clusters. The only experimental studies on metal-doped boron clusters reported prior to this study concern the structure of two Au-doped boron clusters, $Au_2B_7^-$ and AuB_{10}^-, in which the Au atoms are found to behave like H atoms.[25,26] A number of calculations on Al−B mixed clusters have been reported.[27−29] The most relevant work is a report,[27] which suggested that a planar nonacoordinated structure with a central Al atom (D_{9h}) is the global minimum of AlB_9, whereas a decacoordinated (D_{10h}) structure of AlB_{10}^+ corresponds to a local minimum on the potential energy surface. The current study shows that, for AlB_6^- and AlB_{11}^-, the aluminum atom avoids hypercoordination and occupies a peripheral position, inducing planarization to the B_7^- and B_{12}^- parent clusters, respectively.

EXPERIMENTAL AND COMPUTATIONAL METHODS

Photoelectron Spectroscopy. The experiment was performed using a magnetic-bottle PES apparatus equipped with a laser vaporization cluster source, details of which have been published elsewhere.[30] Briefly, the aluminum-doped boron clusters were produced by laser vaporization of a target made of isotopically enriched ^{10}B or ^{11}B (∼10% wt), Al (∼2.5% wt), balanced by Bi or Au, which acted as binders for the targets and provided convenient intrinsic calibrants for the apparatus. The vaporization laser beam (∼10 mJ/pulse, 7 ns pulse width at 532 nm) was focused onto the disk target inside the nozzle. The clusters were entrained by the helium carrier gas supplied by two pulsed valves and underwent a supersonic expansion to form a collimated cluster beam. The cluster composition and cooling were controlled by the time delay between the pulsed valves and the vaporization laser and the resident time of the clusters in the nozzle.[31] To achieve an even higher degree of cluster cooling, some experiments were carried out using a mixture of 5% Ar in He as a carrier gas. This approach has been shown recently to produce cold Au cluster anions.[32]

The anionic clusters were extracted from the cluster beam and analyzed with a time-of-flight mass spectrometer. The clusters of interest (AlB_6^- and AlB_{11}^-) were mass selected and decelerated before being intercepted by a photodetachment laser beam: 193 nm (6.424 eV), 266 nm (4.661 eV), or 355 nm (3.496 eV). Photoelectrons were collected at nearly 100% efficiency by a magnetic bottle and analyzed in a 3.5 m long electron flight tube. Photoelectron spectra were calibrated using the atomic spectra of Bi^- or Au^-.[33,34] The kinetic energy resolution of the magnetic bottle apparatus, $\Delta E/E$, was typically ∼2.5%, that is ∼25 meV for 1 eV electrons.

Computational Methods. The search for the global minimum structures of AlB_6^- and AlB_{11}^- was performed using the Coalescence Kick (CK) method.[35] The CK method subjects large populations of randomly generated structures to a coalescence procedure, in which all atoms are pushed gradually to the center of mass to avoid generation of fragmented structures, and then optimizes them to the nearest local minima. The initial CK global minimum search was performed using the hybrid DFT method known in the literature as B3LYP[36−38] with the small split-valence basis set 3-21G.[39] The structures of all the revealed low-lying isomers were then reoptimized with subsequent frequency calculations at the B3LYP level of theory using the 6-311+G* basis set.[40−43] Single-point energy calculations for the lowest energy isomers of both AlB_6^- and AlB_{11}^- were performed using the restricted (unrestricted) coupled cluster method with single, double, and noniterative triple excitations [R(U)CCSD(T)][44−47] with the 6-311+G(2df) basis set at the geometries optimized at B3LYP/6-311+G*.

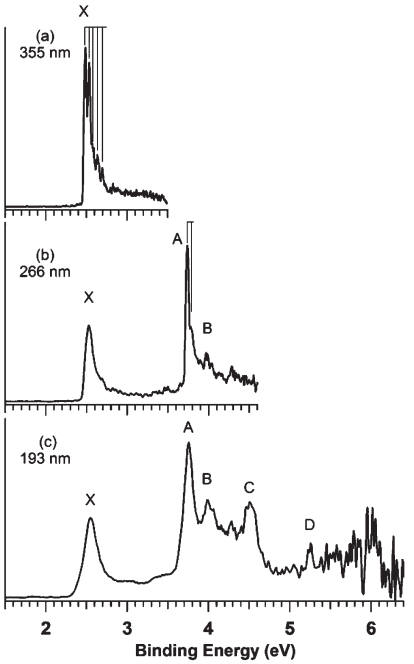

Figure 1. Photoelectron spectra of AlB_6^- at (a) 355 nm (3.496 eV), (b) 266 nm (4.661 eV), and (c) 193 nm (6.424 eV). Vertical lines in (a) and (b) represent resolved vibrational structures.

The vertical detachment energies (VDEs) were calculated using two levels of theory: 1) the time-dependent DFT method[48,49] utilizing the B3LYP functional with the 6-311+G(2df) basis set at the geometries optimized at B3LYP/6-311+G* (TD-B3LYP); 2) the restricted (unrestricted) CCSD(T) calculations with the 6-311+G(2df) basis set at the geometries optimized at B3LYP/6-311+G*. In the TD-B3LYP approach, the first VDE of the global minimum of AlB_6^- was calculated as the lowest transition from the singlet state of the AlB_6^- anion into the final lowest doublet state of neutral AlB_6 at the B3LYP/6-311+G-(2df) level of theory at the geometry optimized for the AlB_6^- anion at B3LYP/6-311+G* (B3LYP/6-311+G(2df)//B3LYP/6-311+G*). Then the vertical excitation energies of neutral AlB_6 were calculated at the TD-B3LYP level at the optimized geometry of the AlB_6^- anion and were added to the first VDE to obtain the higher VDEs of AlB_6^-. The first two VDEs of AlB_{11}^- were calculated at the B3LYP/6-311+G(2df)//B3LYP/6-311+G* level of theory as the lowest transitions from the doublet ground state of the AlB_{11}^- anion into the final lowest singlet and triplet states of neutral AlB_{11} at the geometry optimized for the AlB_{11}^- anion. Then the vertical excitation energies calculated at the TD-B3LYP level for the singlet and triplet states of neutral AlB_{11} were added correspondingly to the two lowest VDEs to obtain the higher VDEs of the AlB_{11}^- anion. Core electrons were frozen in treating the electron correlation at the CCSD(T) level of theory.

Chemical bonding analysis was performed using the adaptive natural density partitioning (AdNDP) method[23,50,51] at B3LYP/3-21G level using the optimized B3LYP/6-311+G* geometries. It has been shown that the results of the AdNDP analysis do not depend much on the level of theory or basis set used.[23,52] All the calculations were performed using the *Gaussian 03* software package.[53] Molecular structure visualization was done using *MOLDEN 3.4*.[54] Molecular orbital visualization was performed using Molekel 4.3.[55]

EXPERIMENTAL RESULTS

The photoelectron spectra of AlB_6^- and AlB_{11}^- are shown in Figures 1 and 2, respectively, each at three different photodetachment energies. The spectra measured at 193 nm reveal spectral features with

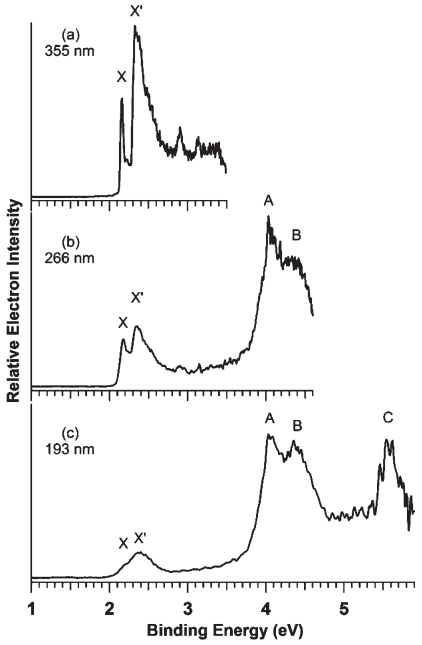

Figure 2. Photoelectron spectra of AlB_{11}^- at (a) 355 nm, (b) 266 nm, and (c) 193 nm.

binding energies up to 6.424 eV, whereas the spectra obtained at lower photon energies offer better spectral resolution. The electronic transitions are labeled with letters and the measured vertical detachment energies (VDE) are given in Tables 1 and 2. The band marked as X usually represents the transition from the ground electronic state of the anion to that of the neutral species, while the higher binding energy bands (A, B, ...) denote transitions to excited electronic states of the neutral cluster.

AlB_6^-. The 355 nm spectrum (part a of Figure 1) shows a vibrationally resolved ground-state transition. The short vibrational progression, with an average spacing of 480 ± 40 cm^{-1}, and the sharp onset of the X band suggest a minimal geometry change upon photodetachment of an electron from the highest occupied molecular orbital (HOMO) of the anion. The intense 0−0 vibrational peak of the X band defines an adiabatic detachment energy (ADE) of 2.49 ± 0.03 eV, which also represents the electron affinity (EA) of neutral AlB_6. Because of the small geometry change between the ground state of AlB_6^- and AlB_6, the VDE and the ADE are the same.

The 266 nm spectrum (part b of Figure 1) reveals two additional PES bands (A and B), corresponding to the two lowest-lying electronic excited states of AlB_6. The A band (ADE = 3.74 ± 0.03 eV) is sharp and intense with a very short vibrational progression, which yields a vibrational frequency of 400 ± 50 cm^{-1} for the first excited state of AlB_6. The A−X energy gap is similar to that observed for the main isomer of the B_7^- cluster (1.2 eV), as reported in ref 15. The B band (VDE, 3.98 ± 0.05 eV) is relatively weak, but its intensity is enhanced in the 193 nm spectrum (part c of Figure 1). There is a weak feature around 4.3 eV (unmarked) in the 266 nm spectrum, whose relative intensity is also enhanced at 193 nm. A relatively intense band C is observed with a VDE of 4.61 ± 0.06 eV in the 193 nm spectrum (part c of Figure 1). There seem to be signals beyond 5 eV, but the signal-to-noise ratios in the higher binding energy side of the 193 nm spectrum are poor. Only one feature D is tentatively labeled at a VDE of 5.26 ± 0.05 eV.

AlB_{11}^-. At 355 nm (part a of Figure 2), two intense bands are observed for AlB_{11}^-. A very sharp band (X) is observed at the threshold with a discernible vibrational feature, yielding an ADE of 2.16 ± 0.03 eV. The second band (X′) with an ADE of 2.33 ± 0.03 eV exhibits a sharp rise and is rather broad. For both the X and X′ bands, their VDEs are the same as their ADEs because of the relatively small geometry changes between the anion and the neutral states, in particular for the X band. There are two weak, but sharp and well resolved features (unmarked) at 2.90 and 3.15 eV in the 355 nm spectrum. However, the relative intensities of these two features seem to decrease with the photon energies, and become negligible in the 193 nm spectrum (part c of Figure 2).

Following a large energy gap, the 266 nm spectrum (part b of Figure 2) displays two broad bands, A and B, with VDEs of 4.06 ± 0.05 eV and 4.38 ± 0.05 eV, respectively. At 193 nm (part c of Figure 2), one more band is observed at the high binding energy side (C, VDE = 5.57 ± 0.05 eV). The parent B_{12} cluster is a highly stable quasiplanar cluster with a large HOMO−LUMO gap, as revealed from the PES spectra of B_{12}^-.[12] The PES patterns of AlB_{11}^- are similar to those of B_{12}^-, except the fact that there are two strong features (X and X′) in the low binding energy range. These features suggest the presence of low-lying isomers, which are borne out from the theoretical calculations (vide infra). We note that the two unmarked weak features observed in the 355 nm (part a of Figure 2) occur in the HOMO−LUMO gap region, as will be shown later. We observe these features with both ^{10}B and ^{11}B isotopes, ruling out contributions from impurities. We attribute tentatively these weak features to multielectron (shakeup) transitions.

Table 1. Comparison of the Experimental VDEs with the Calculated Values for Structure I (C_s, $^1A'$) of AlB_6^-, All Energies Are in eV

			VDE (theor)	
feature	VDE (exptl)[a]	final state and electronic configuration	TD-B3LYP[b]	CCSD(T)[c]
X	2.49(3)	$^2A''$, {...4a′²5a′²3a″²4a″²6a′²5a″¹}	2.30	2.52
A	3.74(3)	$^2A'$, {...4a′²5a′²3a″²4a″²6a′¹5a″²}	3.79	3.80
B	3.98(4)	$^2A''$, {...4a′²5a′²3a″²4a″¹6a′²5a″²}	4.04	[e]
C	4.51(4)	$^2A''$, {...4a′²5a′²3a″¹4a″²6a′²5a″²}	4.48	[e]
D	5.26(4)	$^2A'$, {...4a′²5a′¹3a″²4a″²6a′²5a″²}	5.43[d]	[e]
		$^2A'$, {...4a′¹5a′²3a″²4a″²6a′²5a″²}	5.93[d]	[e]

[a] Numbers in parentheses represent the uncertainty in the last digit. [b] VDEs were calculated at the TD-B3LYP/6-311+G(2df)//B3LYP/6-311+G* level of theory. [c] VDEs were calculated at the R(U)CCSD(T)/6-311+G(2df)//B3LYP/6-311+G* level of theory. [d] VDE corresponds to transition of multiconfigurational nature. [e] VDE value cannot be calculated at this level of theory.

THEORETICAL RESULTS

AlB_6^-. Figure 3 presents the global minimum and all other isomers of AlB_6^-, which were initially found using the CK global minimum search at the B3LYP/3-21G level of theory. All the structures were reoptimized at the B3LYP/6-311+G* level of theory with subsequent frequency calculations. The global minimum of AlB_6^- was identified as **I** (C_s, $^1A'$), which has a nearly planar hexagonal structure (Figure 3). Four low-lying isomers (ΔE < 3 kcal/mol) were found at the B3LYP/6-311+G* level of theory: **III** (ΔE = 0.2 kcal/mol), **VII** (ΔE = 1.4 kcal/mol), **VI** (ΔE = 1.6 kcal/mol), and **V** (ΔE = 2.6 kcal/mol). To determine the proper order of the isomers we performed single-point energy calculations at a higher level of theory (CCSD(T)/6-311+G(2df) //B3LYP/6-311+G*) for all isomers lying within 20 kcal/mol of the global minimum at the B3LYP/6-311+G* level of theory. The isomers shown in Figure 3 are arranged and

Table 2. Comparison of the Experimental VDEs with the Calculated Values for Structures XIX (C_{2v}, $^2A_2$) and XX (C_{2v}, $^2B_1$) of AlB_{11}^-, All Energies Are in eV

			VDE (theor)	
feature	VDE (exptl)[a]	final state and electronic configuration	TD-B3LYP[b]	CCSD(T)[c]
		Isomer XIX		
X	2.16(3)	$^1A_1$, {...$7a_1^2 5b_2^2 8a_1^2 1a_2^2 2b_1^2 6b_2^2 9a_1^2 2a_2^0$}	2.04	2.08
A	4.06(5)	$^3A_2$, {...$7a_1^2 5b_2^2 8a_1^2 1a_2^2 2b_1^2 6b_2^2 9a_1^1 2a_2^1$}	4.00	4.14
		$^1A_2$, {...$7a_1^2 5b_2^2 8a_1^2 1a_2^2 2b_1^2 6b_2^2 9a_1^1 2a_2^1$}	4.11	[e]
B	4.38(5)	$^3B_1$, {...$7a_1^2 5b_2^2 8a_1^2 1a_2^2 2b_1^2 6b_2^1 9a_1^2 2a_2^1$}	4.42	4.51
		$^3B_2$, {...$7a_1^2 5b_2^2 8a_1^2 1a_2^2 2b_1^1 6b_2^2 9a_1^2 2a_2^1$}	4.53	4.75
		$^1B_1$, {...$7a_1^2 5b_2^2 8a_1^2 1a_2^2 2b_1^2 6b_2^1 9a_1^2 2a_2^1$}	4.62	[e]
		$^3A_1$, {...$7a_1^2 5b_2^2 8a_1^2 1a_2^1 2b_1^2 6b_2^2 9a_1^2 2a_2^1$}	4.89	5.10
		$^1B_2$, {...$7a_1^2 5b_2^2 8a_1^2 1a_2^2 2b_1^1 6b_2^2 9a_1^2 2a_2^1$}	5.11	[e]
C	5.57(5)	$^3A_2$, {...$7a_1^2 5b_2^2 8a_1^1 1a_2^2 2b_1^2 6b_2^2 9a_1^2 2a_2^1$}	5.50	[e]
		$^1A_1$, {...$7a_1^2 5b_2^2 8a_1^2 1a_2^1 2b_1^2 6b_2^2 9a_1^2 2a_2^1$}	5.51[d]	[e]
		$^1A_2$, {...$7a_1^2 5b_2^2 8a_1^1 1a_2^2 2b_1^2 6b_2^2 9a_1^2 2a_2^1$}	5.65	[e]
		$^3B_1$, {...$7a_1^2 5b_2^1 8a_1^2 1a_2^2 2b_1^2 6b_2^2 9a_1^2 2a_2^1$}	5.95	[e]
		$^3A_2$, {...$7a_1^1 5b_2^2 8a_1^2 1a_2^2 2b_1^2 6b_2^2 9a_1^2 2a_2^1$}	5.97	[e]
		$^1B_1$, {...$7a_1^2 5b_2^1 8a_1^2 1a_2^2 2b_1^2 6b_2^2 9a_1^2 2a_2^1$}	6.10[d]	[e]
		Isomer XX		
X′	2.33(3)	$^1A_1$, {...$8a_1^2 1a_2^2 6b_2^2 2b_1^2 9a_1^2 3b_1^0$}	2.20	2.24
		$^1B_1$, {...$8a_1^2 1a_2^2 6b_2^2 2b_1^2 9a_1^1 3b_1^1$}	4.02	[e]
		$^3B_1$, {...$8a_1^2 1a_2^2 6b_2^2 2b_1^2 9a_1^1 3b_1^1$}	4.08	4.19
		$^3A_1$, {...$8a_1^2 1a_2^2 6b_2^2 2b_1^1 9a_1^2 3b_1^1$}	4.18	4.34
		$^3A_2$, {...$8a_1^2 1a_2^2 6b_2^1 2b_1^2 9a_1^2 3b_1^1$}	4.23	4.30
		$^1A_1$, {...$8a_1^2 1a_2^2 6b_2^2 2b_1^1 9a_1^2 3b_1^1$}	4.75	[e]
		$^3B_2$, {...$8a_1^2 1a_2^1 6b_2^2 2b_1^2 9a_1^2 3b_1^1$}	5.27	
		$^3B_1$, {...$8a_1^1 1a_2^2 6b_2^2 2b_1^2 9a_1^2 3b_1^1$}	5.55	[e]
		$^1B_1$, {...$8a_1^1 1a_2^2 6b_2^2 2b_1^2 9a_1^2 3b_1^1$}	5.69	[e]
		$^1B_2$, {...$8a_1^2 1a_2^1 6b_2^2 2b_1^2 9a_1^2 3b_1^1$}	6.06[d]	[e]

[a] Numbers in parentheses represent the uncertainty in the last digit. [b] VDEs were calculated at TD-B3LYP/6-311+G(2df)//B3LYP/6-311+G* level of theory. [c] VDEs were calculated at CCSD(T)/6-311+G(2df)//B3LYP/6-311+G* level of theory. [d] VDE corresponds to transition of multiconfigurational nature. [e] VDE value cannot be calculated at this level of theory.

enumerated according to the relative energies calculated at the CCSD(T) level. The relative energies of **III**, **VII**, **VI**, and **V** increased considerably (ΔE > 5 kcal/mol) at the CCSD(T) level as compared to the B3LYP/6-311+G* level, whereas the relative energy of **II** decreased from 7.5 kcal/mol (B3LYP) to 4.2 kcal/mol (CCSD(T)). The structures of AlB_6^- containing a planar tetra- (**VIII**), penta- (**X**), and hexacoordinate (**XVI**) aluminum atom were found to be high-lying isomers.

AlB_{11}^-. Figure 4 shows all structures of AlB_{11}^- obtained from the CK global minimum search up to 42 kcal/mol above the global minimum. Again all of the isomers of AlB_{11}^- were reoptimized at the B3LYP/6-311+G* level along with frequency calculations. There are only three low-lying isomers for AlB_{11}^- at the B3LYP/6-311+G* level of theory: **XX** (ΔE = 0.0 kcal/mol), **XIX** (ΔE = 2.3 kcal/mol), and **XXI** (ΔE = 4.4 kcal/mol); all of the other structures are much higher in energy by more than 14 kcal/mol above the lowest energy structure. The three low-lying isomers were further calculated at UCCSD(T)/6-311+G(2df)//B3LYP/6-311+G* and they are ordered accordingly in Figure 4. At the CCSD(T) level, isomer **XIX** is the global minimum, which has a perfect planar structure and can be viewed as replacing a peripheral B atom from the C_{3v} B_{12}.[12] Isomer **XX**, which can be viewed as an Al atom attached to one edge of the planar B_{11} cluster,[12] is only 1.0 kcal/mol higher in energy at the CCSD(T) level and is competing for the global minimum. Isomer **XXI** is 3.9 kcal/mol higher in energy at the CCSD(T) level and it can be viewed as replacing a B atom from the peripheral of the C_{3v} B_{12}, but at a different position from that of the global minimum **XIX**. Isomers in which the Al is inside the planar structures are much higher in energy (see **XXII**, **XXVII**, and **XXIX** in Figure 4) and are not viable structures.

■ COMPARISON BETWEEN EXPERIMENTAL AND THEORETICAL RESULTS

AlB_6^-. According to the relative energies calculated at the CCSD(T) level, the global minimum **I** of AlB_6^- is significantly more stable than the nearest low-lying isomer **II**. Because our cluster source is relatively cold, as evidenced by the absence of any measurable hot band transitions (part a of Figure 1), we can rule out any significant contributions to the PES spectra of AlB_6^- from low-lying isomers. As will be shown below, the main spectral features are in good agreement with the theoretical results from the lowest energy isomer **I**.

dx.doi.org/10.1021/ja2012438 |J. Am. Chem. Soc. 2011, 133, 8646–8653

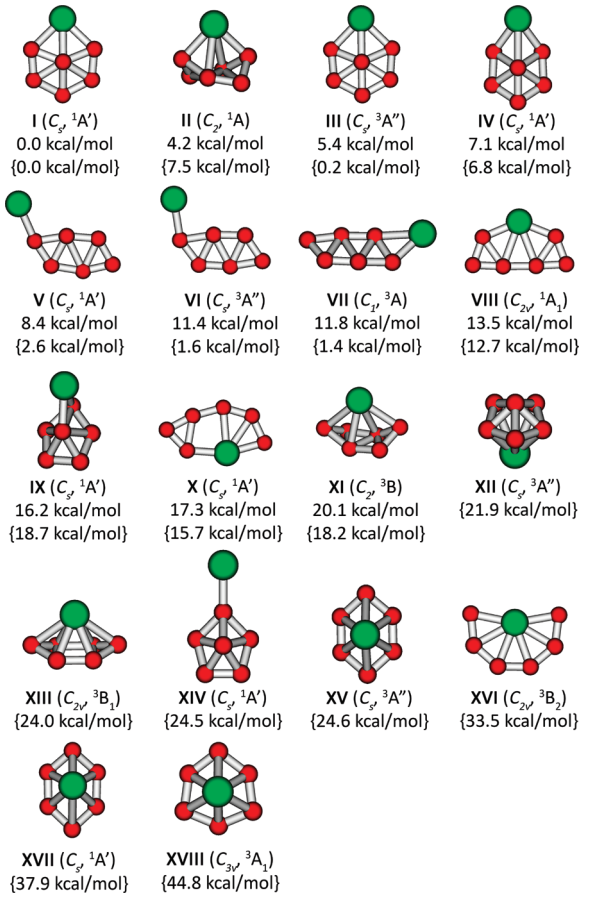

Figure 3. Optimized structures for AlB_6^-, their point group symmetries, spectroscopic states, and relative energies. Relative energies are given at CCSD(T)/6-311+G(2df)//B3LYP/6-311+G* and at B3LYP/6-311+G* (in curly brackets). All the relative energies have been corrected for zero-point energies calculated at the B3LYP/6-311+G* level.

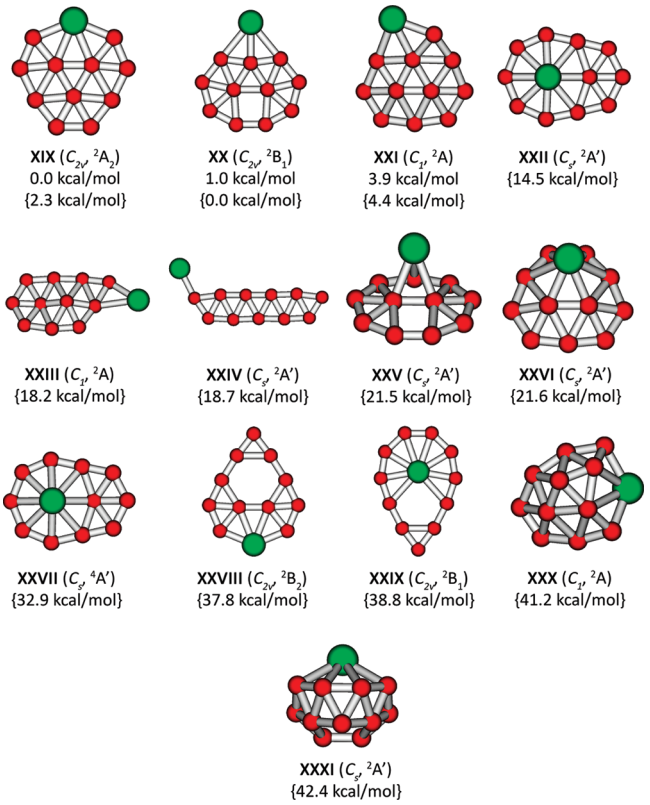

Figure 4. Optimized structures for AlB_{11}^-, their point group symmetries, spectroscopic states, and relative energies. Relative energies are given at CCSD(T)/6-311+G(2df)//B3LYP/6-311+G* and at B3LYP/6-311+G* (in curly brackets). All the relative energies have been corrected for zero-point energies calculated at the B3LYP/6-311+G* level.

The global minimum of AlB_6^- is closed shell with a singlet ground state (C_s, ^{1}A′). Thus, each occupied valence MO is expected to yield one PES band, resulting in a doublet final neutral state. The comparison with the calculated VDEs from the global minimum **I** is given in Table 1. The first VDE corresponds to electron detachment from the doubly occupied HOMO (5a″) to produce the final doublet state (^{2}A″) of neutral AlB_6. The calculated VDE at the CCSD(T) level (2.52 eV) is in excellent agreement with the experimental value of 2.49 eV. The first VDE calculated at TD-B3LYP is somewhat lower compared to the experimental data. The second, third, and fourth VDEs correspond to electron detachment from HOMO-1 (6a′), HOMO-2 (4a″), and HOMO-3 (3a″) of the AlB_6^- anion into the final ^{2}A′, ^{2}A″, and ^{2}A″ excited states of neutral AlB_6, respectively (Table 1). The calculated second VDE at the CCSD(T) level (3.80 eV), as well as at TD-B3LYP (3.79 eV), is in excellent agreement with the experimental value (3.74 eV) from the A band. We were not able to compute higher VDEs at the CCSD(T) level. However, the third and fourth VDEs (4.04 and 4.48 eV) from TD-B3LYP are in good agreement with the VDEs from the B band (3.98 eV) and the C band (4.51 eV), respectively. There are two more detachment channels with VDEs around 5.43 and 5.93 eV from TD-B3LYP (Table 1). Because of poor signal-to-noise ratios in the higher binding energy range in the 193 nm spectrum (part c of Figure 1), we cannot definitely assign these two transitions. But they are certainly consistent with the broad features in this spectral range. The unmarked weak feature observed around 4.3 eV does not correspond to any computed detachment channel and it is likely due to a multielectron (shakeup) transition.

We also calculated the VDEs of isomers **II** and **III** (Tables S1 and S2 of the Supporting Information). The calculated VDEs of isomer **II** do not agree with the experimental values. Isomer **III** corresponds to the triplet excited state of the global minimum **I** and yields a slightly lower VDE (2.43 eV) as expected. However, our PES data are very clean in the low binding energy range (Figure 1), ruling out any contribution from isomer **III**. Hence, the excellent agreement between the experimental and theoretical data confirms unequivocally that isomer **I** is the global minimum of AlB_6^-.

AlB_{11}^-. As shown in Figure 4, isomers **XIX** and **XX** of AlB_{11}^- are within 1.0 kcal/mol of each other at the CCSD(T) level and should be considered degenerate within the accuracy of the theory. Thus, both isomers are expected to be present in our cluster beam and contribute to the observed PES spectra. Isomer **XXI** is 3.9 kcal/mol higher in energy at CCSD(T) and is not expected to have any significant population in the cluster beam.

The calculated VDEs for isomers **XIX** and **XX** are compared with the experimental data in Table 2. Both isomers give rise to rather low first VDEs because of the fact that the corresponding neutral clusters are both closed-shell with large HOMO−LUMO

dx.doi.org/10.1021/ja2012438 |J. Am. Chem. Soc. 2011, 133, 8646–8653

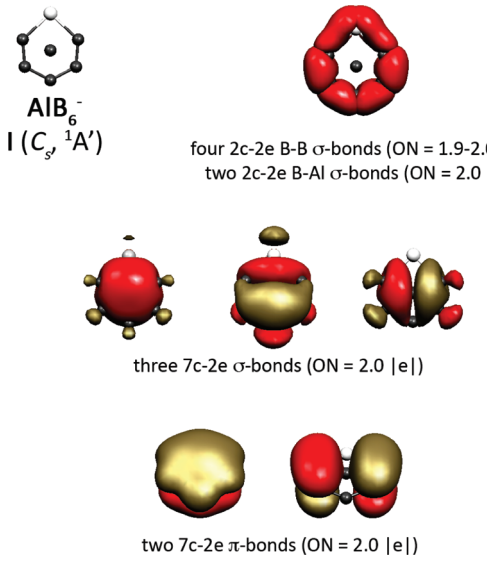

Figure 5. Chemical bonding analysis for the global minimum of AlB_6^- (isomer **I**, C_s, $^1A'$) at the AdNDP/B3LYP/3-21G//B3LYP/6-311+G* level.

gaps. The theoretical VDEs for the two isomers are in excellent agreement with the experimental observations. The first VDE calculated for **XIX** at CCSD(T) is 2.08 eV, slightly smaller than that for **XX** at 2.24 eV. Thus, the lowest X band observed in the PES spectra should come from **XIX**. The experimental VDE of 2.16 eV agrees well with the calculated value of 2.08 eV (Table 2). The next detachment channel for the **XIX** isomer comes from the doubly occupied $9a_1$ orbital, yielding a triplet ($^3A_2$) excited state of the corresponding neutral AlB_{11}. The VDE calculated for this channel at CCSD(T) (4.14 eV) is in good agreement with the VDE of the A band (4.06 eV). The experimental HOMO−LUMO gap (1.90 eV) defined by the X−A VDE difference is also in reasonable agreement with the calculated value of 2.06 eV. There is a high density of detachment channels due to the large size of the AlB_{11}^- cluster and the fact that both triplet and singlet final states are produced. The calculated spectral pattern is in good agreement with the congested spectral features in the high binding energy side. We note that the VDE of **XIX** (2.16 eV) is very similar to that of the parent B_{12}^- (2.26 eV).[12] The HOMO−LUMO gap of **XIX** (1.90 eV) is also similar to that of B_{12}^- (2.05 eV). However, the X band of **XIX** is very sharp in comparison to the first band in the PES spectra of B_{12}^-, suggesting the planar AlB_{12}^- is extremely rigid with little geometry change between the ground states of the anion and the neutral.

The calculated first VDE for **XX** at CCSD(T) is 2.24 eV, which agrees well with the VDE of the X′ band (2.33 eV). The next detachment channel should be from the doubly occupied $9a_1$ orbital, similar to **XIX**, leading to the first triplet excited state ($^3B_1$) of the corresponding neutral. The calculated VDE for this channel at CCSD(T) is 4.19 eV, which overlaps with the A band of **XIX**. There is also a relatively high density of detachment channels for **XX**, which all overlap with those of **XIX**. We further calculated the VDEs for **XXI**, as shown in Table S3 of the Supporting Information. Its first VDE was calculated at 2.27 eV, which may contribute to the X′ band. The second and higher detachment channels for **XXI** all overlap with those of **XIX** and **XX**. On the basis of the energetics, however, we expect the contributions of **XXI** to the PES spectra of AlB_{11}^- to be small, if

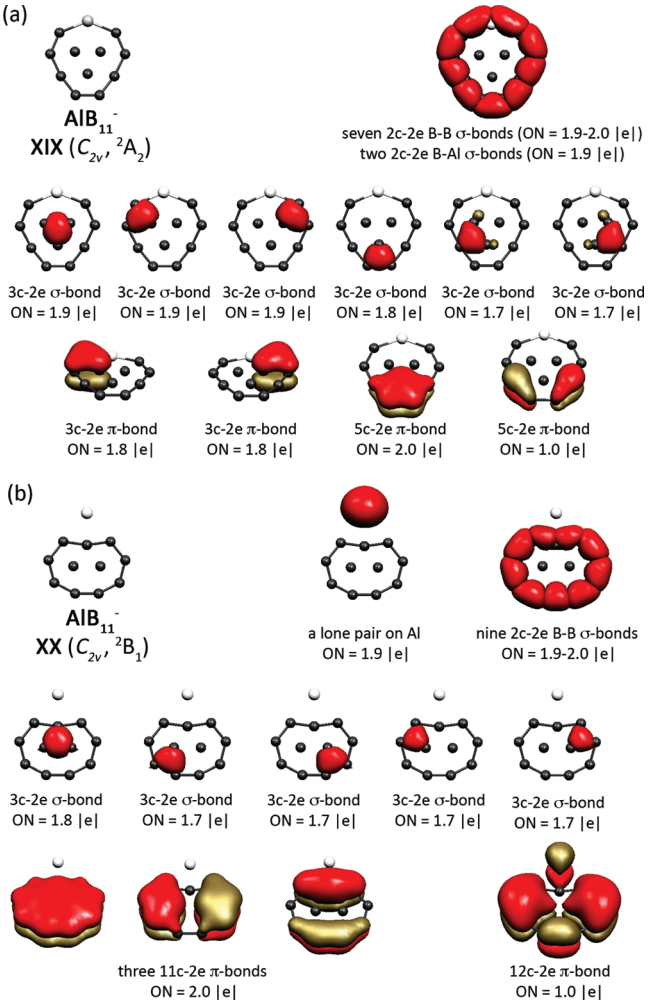

Figure 6. Chemical bonding analysis of the two lowest energy structures of AlB_{11}^- at the AdNDP/B3LYP/3-21G//B3LYP/6-311+G* level: (a) isomer **XIX** (C_{2v}, $^2A_2$), (b) isomer **XX** (C_{2v}, $^2B_1$).

at all. The overall spectral patterns calculated from **XIX** and **XX** are in excellent agreement with the key features of the experimental spectra confirming the presence of the two nearly degenerate isomers for AlB_{11}^-. The two weak features observed at 2.9 and 3.1 eV (part a of Figure 2) occur in the band gap region for all three low-lying isomers of AlB_{11}^- and cannot come from direct one-electron transitions from any of these isomers. They are likely from multielectron (shapeup) processes.

CHEMICAL BONDING ANALYSES AND AL-INDUCED PLANARIZATION

AlB_6^-. The chemical bonding of the global minimum structure of AlB_6^- was analyzed using the AdNDP method, as given in Figure 5. The occupation numbers (denoted as ON) of all the revealed chemical bonds are close to the ideal value of 2.0 |e|. The bonding in AlB_6^- can be explained by the formation of six peripheral 2c−2e σ-bonds: four B−B σ-bonds and two B−Al σ-bonds. The rest of the valence electron density is totally delocalized. There are six delocalized σ-electrons, rendering σ-aromaticity to AlB_6^-, according to the $4n + 2$ rule for aromaticity ($n = 1$). There are four delocalized π-electrons in AlB_6^-, which indicate that AlB_6^- is π-antiaromatic according to the $4n$ rule for antiaromaticity.

dx.doi.org/10.1021/ja2012438 |J. Am. Chem. Soc. 2011, 133, 8646–8653

Therefore, the AlB_6^- cluster is an example of a system with conflicting aromaticity. The π-antiaromatic nature of AlB_6^- explains why this cluster is not perfectly planar, even though the distortion from planarity is very small. The chemical bonding of the global minimum of AlB_6^- is similar to that of the C_{2v} isomer of B_7^- ($^1A_1$).[15] However, AlB_6^- is much closer to a perfect planar structure than its valence isoelectronic B_7^-. Clearly, the large distortion from planarity in B_7^- is due to the fact that the B_6 ring is too small to fit a B atom in its center to from a planar hexagonal structure. Substitution of one B atom by Al at the periphery decreases the geometric strain for planarity because of the slightly bigger AlB_5 ring due to the larger size of Al.

AlB_{11}^-. We performed chemical bonding analyses using AdNDP for the two nearly degenerate isomers **XIX** and **XX** of AlB_{11}^-, as shown in Figure 6. The occupation numbers of all the revealed chemical bonds range from 1.7 to 2.0 |e| for the doubly occupied bonds and are 1.0 |e| for the singly occupied bonds. The current AdNDP method is applicable to closed-shell systems only. Hence, to obtain chemical bonding information for AlB_{11}^-, which has one unpaired electron, we performed AdNDP analyses for the closed-shell AlB_{11}^{2-} and AlB_{11} at the geometry of the singly charged anion. The sets of chemical bonding elements for the doubly charged anion and the neutral species were found to be the same except for one bond, which is not occupied in the neutral species (ON = 0.0 |e|) and was doubly occupied in the doubly charged anion (ON = 2.0 |e|). Thus, we assumed that this bonding element of the singly charged anion should have an occupation number of 1.0 |e|, as shown in Figure 6.

According to the AdNDP analysis, the 19 canonical molecular orbitals for **XIX** can be transformed into the following bonding elements (part a of Figure 6): nine peripheral 2c−2e σ-bonds (seven B−B and two B−Al bonds); two sets of delocalized σ-bonds (one 3c−2e σ-bond delocalized over the inner B_3 triangle and five 3c−2e σ-bonds responsible for bonding between the inner B_3 triangle and the peripheral AlB_8 ring); four delocalized π-bonds (two being doubly occupied and delocalized over three centers, one doubly occupied 5c−2e π-bond, and one singly occupied 5c-1e π-bond). This cluster can be considered as doubly σ-aromatic because the $4n + 2$ rule is satisfied for each set of the σ-bonds: 1) $4n + 2 = 2$ ($n = 0$) for two σ-electrons delocalized over the inner B_3 triangle; 2) $4n + 2 = 10$ ($n = 2$) for the three-center σ-electrons between the inner B_3 ring and the peripheral B atoms. The singly occupied 5c−1e π bond is derived from the extra electron in the anion. Thus, the neutral AlB_{11} corresponding to isomer **XIX** is a highly π-aromatic system with 6π electrons according to the $4n + 2$ rule ($n = 1$). The large HOMO−LUMO gap observed in the PES spectra for XIX suggests the neutral AlB_{11} cluster is a highly stable electronic system consistent with its multiple aromaticity. It is interesting to note that the peripheral Al atom does not seem to participate in any of the delocalized bonding. Thus, in the structure **XIX** presented in Figure 4 it may be more appropriate to omit the bonds between the Al atom and the two inner B atoms.

The chemical bonding pattern of **XIX** is nearly identical to that of its valence isoelectronic B_{12}^- cluster.[12] The structures of these two clusters are similar: a B_3 triangle inside a nine-atom ring. The only difference is that the AlB_{11}^- cluster is perfectly planar, whereas in B_{12}^- the inner B_3 ring is slightly out of plane, giving rise to a bowl-shaped B_{12}^-. Clearly, the B_9 ring is too small to host comfortably the B_3 inner ring in B_{12}^-. Substitution of one B atom in the B_9 ring by the bigger Al atom in AlB_{11}^- gives rise to a slightly larger 9-atom outer ring and a perfectly planar AlB_{11}^- cluster.

The chemical bonding analysis for isomer **XX** of AlB_{11}^- (part b of Figure 6) revealed an Al lone pair, nine 2c−2e B−B σ-bonds, five delocalized 3c−2e σ-bonds, three totally delocalized 11c−2e π-bonds, and one 12c−2e singly occupied π-bond. The latter is derived from the extra electron in the AlB_{11}^- anion. The chemical bonding of **XX** suggests that it is basically an Al atom bonded ionically with a B_{11}^- cluster. We have shown previously that the B_{11}^- cluster is a highly aromatic planar cluster.[12] The B_{11}^- fragment in AlB_{11}^- has little change from the bare B_{11}^- in both its structural details and chemical bonding. Thus, the neutral AlB_{11} corresponding to **XX** can be viewed as $Al^+[B_{11}^-]$.

CONCLUSIONS

We have carried out a joint experimental and theoretical study on the structures and chemical bonding of AlB_6^- and AlB_{11}^- to test if isoelectronic substitution of a B atom by Al in the nonplanar B_7^- and B_{12}^- clusters can induce planarization. Well-resolved photoelectron spectra were obtained for AlB_6^- and AlB_{11}^- and were compared with theoretical calculations for the lowest energy structures found from unbiased global minimum searches. The photoelectron spectra of the Al-doped clusters are similar to those of the bare boron clusters, suggesting their structural similarity. Our global minimum search showed that AlB_6^- is a nearly planar and highly stable cluster in good agreement with the experimental data. Two nearly degenerate perfectly planar isomers were found for AlB_{11}^-, which were both present in the experiment. The one which is slightly more favored is the B_{12}^- analogue, in which a peripheral B atom is replaced by an Al atom. The second isomer, which is only 1 kcal/mol higher in energy at CCSD(T), is a structure that can be viewed as an Al atom interacting with a B_{11}^- cluster. The current work shows that the nonplanarity in B_7^- and B_{12}^- is mechanical in nature. Thus, suitable isoelectronic substitution can be a powerful means to elucidate the structures and bonding of complex atomic clusters, as we have shown recently for Cu or Ag substituted Au clusters.[56]

ASSOCIATED CONTENT

Supporting Information. Ref 53 in full, as well as tables containing calculated VDEs for low-lying structures of AlB_6^- (isomers **II** and **III**) and AlB_{11}^- (isomer **XXI**) and the Cartesian coordinates of the three lowest isomers of AlB_6^- and AlB_{11}^-. This material is available free of charge via the Internet at http://pubs.acs.org.

AUTHOR INFORMATION

Corresponding Author
a.i.boldyrev@usu.edu; Lai-Sheng_Wang@brown.edu

ACKNOWLEDGMENT

We thank Dr. Hua-Jin Zhai for help in the early part of the experiment. This research was supported by the National Science Foundation (DMR-0904034 to LSW and CHE-1057746 to A.I.B.). Computer time from the Center for High Performance Computing at Utah State University is gratefully acknowledged. The computational resource, the Uinta cluster supercomputer, was provided through the National Science Foundation under Grant CTS-0321170 with matching funds provided by Utah State University.

REFERENCES

(1) Cotton, F. A.; Wilkinson, G.; Murillo, C. A.; Bochmann, M. *Advanced Inorganic Chemistry*, 6th ed.; Wiley-Interscience: New York, 1999.

(2) (a) Fujimori, M.; Nakata, T.; Nakayama, T.; Nishibori, E.; Kimura, K.; Takata, M.; Sakata, M. *Phys. Rev. Lett.* **1999**, *82*, 4452. (b) Vast, N.; Baroni, S.; Zerah, G.; Besson, J. M.; Polian, A.; Grimsditch, M.; Chervin, J. C. *Phys. Rev. Lett.* **1997**, *78*, 693.

(3) Hanley, L.; Whitten, J. L.; Anderson, S. L. *J. Phys. Chem.* **1988**, *92*, 5803.

(4) (a) Kawai, R.; Weare, J. H. *J. Chem. Phys.* **1991**, *95*, 1151. (b) Kawai, R.; Weare, J. H. *Chem. Phys. Lett.* **1992**, *191*, 311.

(5) (a) Hernandez, R.; Simons, J. *J. Chem. Phys.* **1991**, *94*, 2961. (b) Martin, J. M. L.; François, J. P.; Gijbels, R. *Chem. Phys. Lett.* **1992**, *189*, 529. (c) Kato, H.; Yamashita, K.; Morokuma, K. *Chem. Phys. Lett.* **1992**, *190*, 361.

(6) (a) Boustani, I. *Int. J. Quantum Chem.* **1994**, *52*, 1081. (b) Boustani, I. *Phys. Rev. B* **1997**, *55*, 16426. (c) Boustani, I. *Surf. Sci.* **1997**, *370*, 355. (d) Boustani, I.; Quandt, A. *Comput. Mater. Sci.* **1998**, *11*, 132.

(7) Ricca, A.; Bauschlicher, C. W. *Chem. Phys.* **1996**, *208*, 233.

(8) (a) Niu, J.; Rao, B. K.; Jena, P. *J. Chem. Phys.* **1997**, *107*, 132. (b) Gu, F. L.; Yang, X.; Tang, A. C.; Jiao, H.; Schleyer, P. v. R. *J. Comput. Chem.* **1998**, *19*, 203.

(9) Zhai, H. J.; Wang, L. S.; Alexandrova, A. N.; Boldyrev, A. I. *J. Chem. Phys.* **2002**, *117*, 7917.

(10) Alexandrova, A. N.; Boldyrev, A. I.; Zhai, H. J.; Wang, L. S.; Steiner, E.; Fowler, P. W. *J. Phys. Chem. A* **2003**, *107*, 1359.

(11) Zhai, H. J.; Alexandrova, A. N.; Birch, K. A.; Boldyrev, A. I.; Wang, L. S. *Angew. Chem., Int. Ed. Engl.* **2003**, *42*, 6004.

(12) Zhai, H. J.; Kiran, B.; Li, J.; Wang, L. S. *Nat. Mater.* **2003**, *2*, 827.

(13) Zhai, H. J.; Wang, L. S.; Alexandrova, A. N.; Boldyrev, A. I. *J. Phys. Chem. A* **2003**, *107*, 9319.

(14) Alexandrova, A. N.; Zhai, H. J.; Wang, L. S.; Boldyrev, A. I. *Inorg. Chem.* **2004**, *43*, 3552.

(15) Alexandrova, A. N.; Boldyrev, A. I.; Zhai, H.-J.; Wang, L. S. *J. Phys. Chem. A* **2004**, *108*, 3509.

(16) Kiran, B.; Bulusu, S.; Zhai, H. J.; Yoo, S.; Zeng, X. C.; Wang, L. S. *Proc. Natl. Acad. Sci. U. S. A.* **2005**, *102*, 961.

(17) Alexandrova, A. N.; Boldyrev, A. I.; Zhai, H. J.; Wang, L. S. *J. Chem. Phys.* **2005**, 122.

(18) Alexandrova, A. N.; Boldyrev, A. I.; Zhai, H. J.; Wang, L. S. *Coord. Chem. Rev.* **2006**, *250*, 2811.

(19) Sergeeva, A. P.; Zubarev, D. Y.; Zhai, H. J.; Boldyrev, A. I.; Wang, L. S. *J. Am. Chem. Soc.* **2008**, *130*, 7244.

(20) Pan, L. L.; Li, J.; Wang, L. S. *J. Chem. Phys.* **2008**, *129*, 024302.

(21) Huang, W.; Sergeeva, A. P.; Zhai, H. J.; Averkiev, B. B.; Wang, L. S.; Boldyrev, A. I. *Nat. Chem.* **2010**, *2*, 202.

(22) Zubarev, D. Y.; Boldyrev, A. I. *J. Comput. Chem.* **2007**, *28*, 251.

(23) Zubarev, D. Y.; Boldyrev, A. I. *Phys. Chem. Chem. Phys.* **2008**, *10*, 5207.

(24) Zubarev, D. Y.; Sergeeva, A. P.; Boldyrev, A. I. In *Chemical Reactivity Theory: A Density Functional View*; Chattaraj, P. K., Ed.; CRC Press: 2009; p 439.

(25) Zhai, H. J.; Wang, L. S.; Zubarev, D. Y.; Boldyrev, A. I. *J. Phys. Chem. A* **2006**, *110*, 1689.

(26) Zhai, H. J.; Miao, C. Q.; Li, S. D.; Wang, L. S. *J. Phys. Chem. A* **2010**, *114*, 12155.

(27) Averkiev, B. B.; Boldyrev, A. I. *Russ. J. Gen. Chem.* **2008**, *78*, 769.

(28) Averkiev, B. B.; Wang, L. M.; Huang, W.; Wang, L. S.; Boldyrev, A. I. *Phys. Chem. Chem. Phys.* **2009**, *11*, 9840.

(29) (a) Guo, J. C.; Yao, W. Z.; Li, Z.; Li, S. D. *Sci. China, Ser. B: Chem.* **2009**, *52*, 566. (b) Jiang, Z. Y.; Lou, X. M.; Li., S. T.; Chu, S. Y. *Int. J. Mass Spectrom.* **2006**, *252*, 197. (c) Kawamata, H.; Negishi, Y.; Nakajima, A.; Kaya, K. *Chem. Phys. Lett.* **2001**, *337*, 255. (d) Feng, X. J.; Luo, Y. H. *J. Phys. Chem. A* **2007**, *111*, 2420.

(30) (a) Wang, L. S.; Cheng, H. S.; Fan, J. *J. Chem. Phys.* **1995**, *102*, 9480.(b) Wang, L. S.; Li, X. In *Advances in Metal and Semiconductor Clusters. IV. Cluster Materials*;Duncan, M. A., Ed.; JAI Press: Greenwich, 1998; pp 299−343.

(31) (a) Akola, J.; Manninen, M.; Hakkinen, H.; Landman, U.; Li, X.; Wang, L. S. *Phys. Rev. B* **1999**, *60*, R11297.(b) Wang, L. S.; Li, X. In *Clusters and Nanostructure Interfaces*; Jena, P., Khanna, S. N., Rao, B. K., Eds.; World Scientific: River Edge, NJ, 2000; pp 293−300.

(32) (a) Huang, H.; Wang, L. S. *Phys. Chem. Chem. Phys.* **2009**, *11*, 2663. (b) Huang, W.; Wang, L. S. *Phys. Rev. Lett.* **2009**, *102*, 153401. (c) Huang, H.; Bulusu, S.; Pal, R.; Zeng, X. C.; Wang, L. S. *ACS Nano* **2009**, *3*, 1225.

(33) Bilodeau, R. C.; Haugen, H. K. *Phys. Rev. A* **2001**, *64*, 024501.

(34) Feigerle, C. S.; Corderman, R. R.; Bobashev, S. V.; Lineberger, W. C. *J. Chem. Phys.* **1981**, *74*, 1580.

(35) Averkiev, B. B., Ph.D. thesis, Utah State University, Logan, UT, 2009.

(36) Becke, A. D. *J. Chem. Phys.* **1993**, *98*, 5648.

(37) Vosko, S. H.; Wilk, L.; Nusair, M. *Can. J. Phys.* **1980**, *58*, 1200.

(38) Lee, C. T.; Yang, W. T.; Parr, R. G. *Phys. Rev. B* **1988**, *37*, 785.

(39) Binkley, J. S.; Pople, J. A.; Hehre, W. J. *J. Am. Chem. Soc.* **1980**, *102*, 939.

(40) Gordon, M. S.; Binkley, J. S.; Pople, J. A.; Pietro, W. J.; Hehre, W. J. *J. Am. Chem. Soc.* **1982**, *104*, 2797.

(41) Pietro, W. J.; Francl, M. M.; Hehre, W. J.; Defrees, D. J.; Pople, J. A.; Binkley, J. S. *J. Am. Chem. Soc.* **1982**, *104*, 5039.

(42) McLean, A. D.; Chandler, G. S. *J. Chem. Phys.* **1980**, *72*, 5639.

(43) Clark, T.; Chandrasekhar, J.; Spitznagel, G. W.; Schleyer, P. v. R. *J. Comput. Chem.* **1983**, *4*, 294.

(44) Cizek, J. *Adv. Chem. Phys.* **1969**, *14*, 35.

(45) Purvis, G. D.; Bartlett, R. J. *J. Chem. Phys.* **1982**, *76*, 1910.

(46) Raghavachari, K.; Trucks, G. W.; Pople, J. A.; Headgordon, M. *Chem. Phys. Lett.* **1989**, *157*, 479.

(47) Knowles, P. J.; Hampel, C.; Werner, H. J. *J. Chem. Phys.* **1993**, *99*, 5219.

(48) Bauernschmitt, R.; Ahlrichs, R. *Chem. Phys. Lett.* **1996**, *256*, 454.

(49) Casida, M. E.; Jamorski, C.; Casida, K. C.; Salahub, D. R. *J. Chem. Phys.* **1998**, *108*, 4439.

(50) Zubarev, D. Y.; Boldyrev, A. I. *J. Org. Chem.* **2008**, *73*, 9251.

(51) Zubarev, D. Y.; Boldyrev, A. I. *J. Phys. Chem. A* **2009**, *113*, 866.

(52) Sergeeva, A. P.; Boldyrev, A. I. *Comments Inorg. Chem.* **2010**, *31*, 2.

(53) Frisch, M. J. et al. . *Gaussian 03*, revision D.01; Gaussian, Inc.: Wallingford, CT, 2004.

(54) Schaftenaar, G. *MOLDEN3.4*, CAOS/CAMM Center, The Netherlands, 1998.

(55) Portmann, S. Molekel, Version 4.3. Swiss National Supercomputing Centre/Swiss Federal Institute of Technology, Zurich, 2002.

(56) (a) Huang, W.; Pal, R.; Wang, L. M.; Zeng, X. C.; Wang, L. S. *J. Chem. Phys.* **2010**, *132*, 054305. (b) Wang, L. M.; Pal, R.; Huang, W.; Zeng, X. C.; Wang, L. S. *J. Chem. Phys.* **2010**, *132*, 114306. (c) Pal, R.; Wang, L. M.; Huang, W.; Wang, L. S.; Zeng, X. C. *J. Chem. Phys.* **2011**, *134*, 054306.